Electronic Supplementary Material (ESI) for Chemical Science.
This journal is © The Royal Society of Chemistry 2019

Electronic Supplementary Information

Understanding of the multiscale self-assembly of metal-organic polyhedra towards functionally graded porous gels

Alexandre Legrand,[a] Gavin A. Craig,[a] Mickaele Bonneau,[a] Saori Minami,[b] Kenji Urayama,[b] Shuhei Furukawa[a,c,*]

[a]Institute for Integrated Cell-Material Sciences (WPI-iCeMS), Kyoto University, Yoshida, Sakyo-ku, Kyoto 606-8501, Japan

[b]Department of Macromolecular Science and Engineering, Kyoto Institute of Technology, Matsugasaki, Sakyo-ku, Kyoto 606-8585, Japan

[c]Department of Synthetic Chemistry and Biological Chemistry, Graduate School of Engineering, Kyoto University, Katsura, Nishikyo-ku, Kyoto 615-8510, Japan

*To whom correspondence should be addressed: shuhei.furukawa@icems.kyoto-u.ac.jp

Theory Background of dynamic light scattering (DLS)

In DLS, the time-intensity correlation function (ICF) allows the time dependence of the diffusion of the scattering elements in the presence of noise to be extracted. The function represents the delay, in µs, necessary for the diffusion speed of scattering particles to decay after interacting with incident light. In the solution state the ICF is best described by the sum of a single and stretched exponential functions:

$$g^{(2)}(\tau) - 1 = \sigma_1^2 \left\{ A e^{(-\tau/\tau_f)} + (1 - A) e^{-(\tau/\tau_s)^{\beta}} \right\}^2 \quad (1)$$

σ_1^2 is the initial amplitude of ICF with values close to the instrumental coherence factor (usually ≈1). During the gelation process, the system tends towards nonergodicity resulting in a decrease in σ_1^2. A (0 < A < 1) is the fraction of the collective diffusion mode. β ($0 < \beta < 1$) is the stretched exponent and reflects the distribution of relaxation times of the slow mode. τ_f and τ_s are the characteristic relaxation times of the fast and slow modes respectively. τ_f is also called the gel mode and is related to the collective diffusion of local motions, D, by:

$$\tau_f = 1/(q^2 D) \quad (2)$$

with q the wave vector defined as*:*

$$q = \frac{4\pi r_i}{\lambda} sin(\theta/2) \qquad (3)$$

where r_i is the refractive solvent index, λ is the incident wavelength and θ is the angle at which the detector is placed. Here, the detector position is fixed at 173° (backscattering mode) to reduce multiple scattering.

The collective diffusion D is also related to the correlation length through the Stokes-Einstein equation:

$$\xi = \frac{k_B T}{6\pi\eta D} \quad (4)$$

with k_B the Boltzmann constant, T the temperature and η the viscosity of the solvent. In polymer gel systems, the correlation length corresponds to the distance between two cross-linked sites (mesh size depicted in Figure S1) and is equivalent in our colloidal gel system to the distance between two branching units.

During the supramolecular polymerization reaction, the particles grow into colloids and their aggregation hinders their free diffusion. Hence, the characteristic times for the decays to start are shifted to higher delay time. At the gelation threshold, the ICF is best described by a single exponential and power law functions:

$$g^{(2)}(\tau) - 1 = \sigma_1^2 \left\{ A e^{(-\tau/\tau_f)} + (1 - A)(1 + \tau/\tau^*)^{(n-1)/2} \right\}^2 \ (5)$$

The change of shape of the ICF is a characteristic feature of gels and is due to the appearance of connectivity divergence as colloids form domains during the dynamic formation of the gel network.

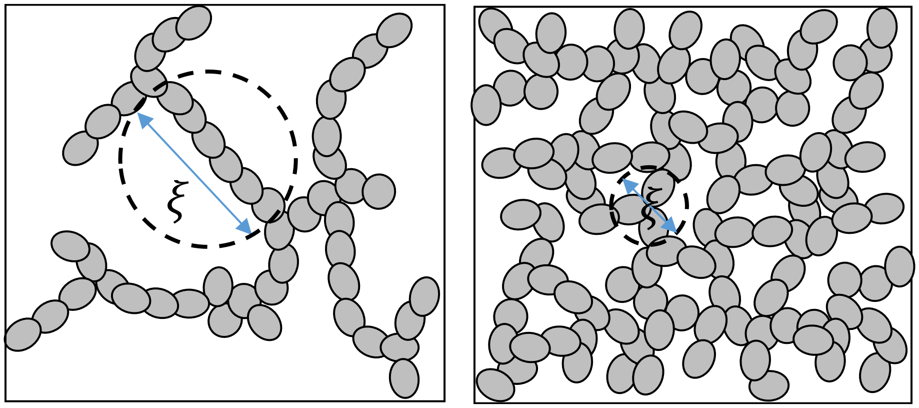

Figure S1. Schematic representation of the correlation length in the case of low (left) and high (right) branching colloidal particle networks.

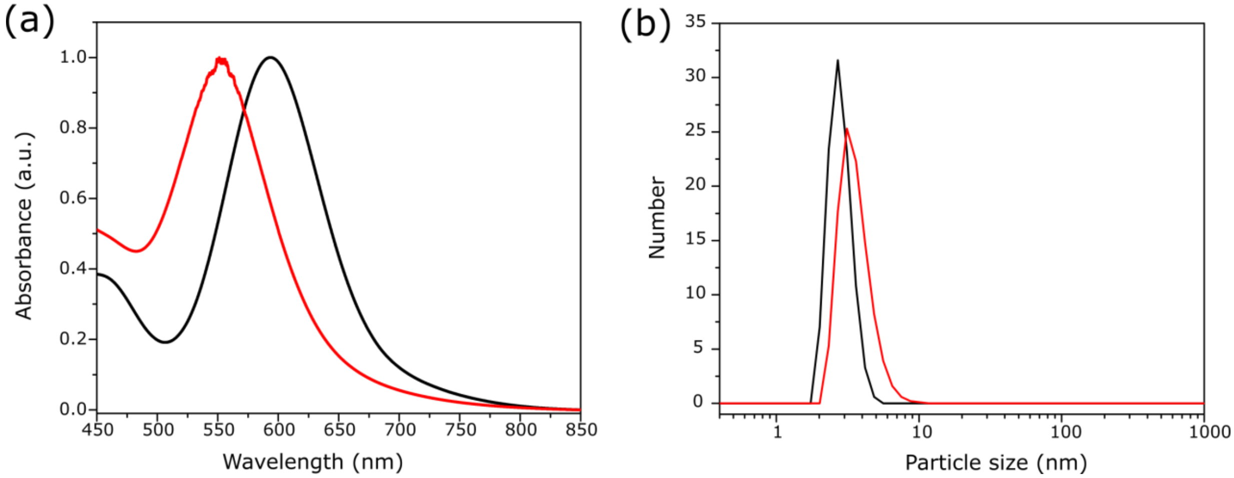

Figure S2. (a) UV-visible spectra of **C_{12}RhMOP** (black) and **(C_{12}RhMOP)(bix)$_{12}$** (red). (b) DLS measurements of **C_{12}RhMOP** (black) and **(C_{12}RhMOP)(bix)$_{12}$** particle size.

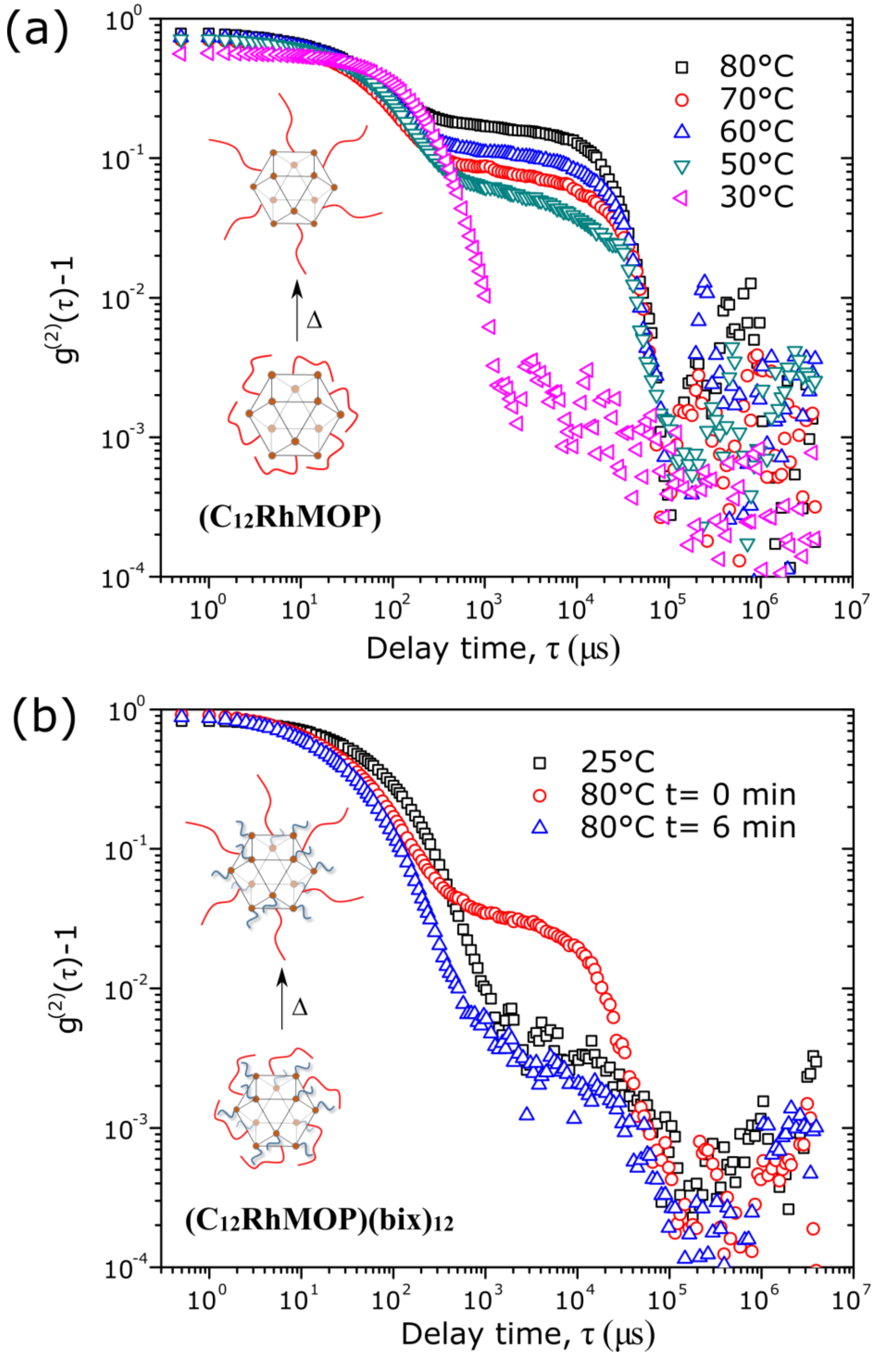

Figure S3. Temperature effect on the ICF decay for (a) 0.93 mM **(C_{12}RhMOP)** in DMF from 30°C to 80°C and (b) 0.93 mM **(C_{12}RhMOP)(bix)$_{12}$** in DMF at 25°C and 80°C at the beginning of the reaction and after 6 min. Both show the appearance of a 2nd relaxation time at higher temperature. The one of **(C_{12}RhMOP)(bix)$_{12}$** decrease after 6 min of reaction at 80°C. The scheme (inset) is the possible mechanism explaining the variation observed in the ICF, which is the thermal agitation of the extended C12 alkyl chains of the MOP's linkers (in red).

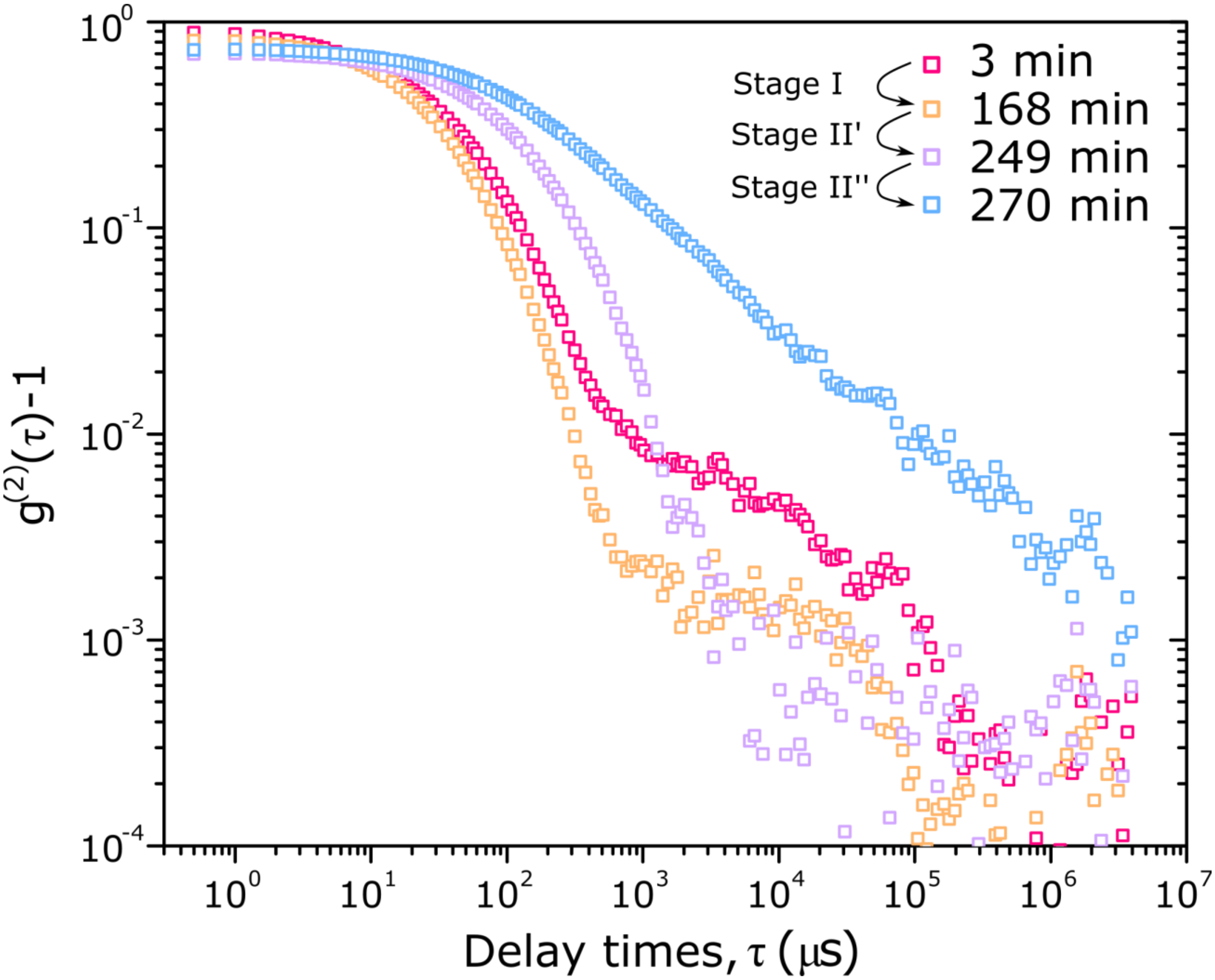

Figure S4. Variation of ICF as function of characteristic reaction time representative of transition between the different stages of the gelation process.

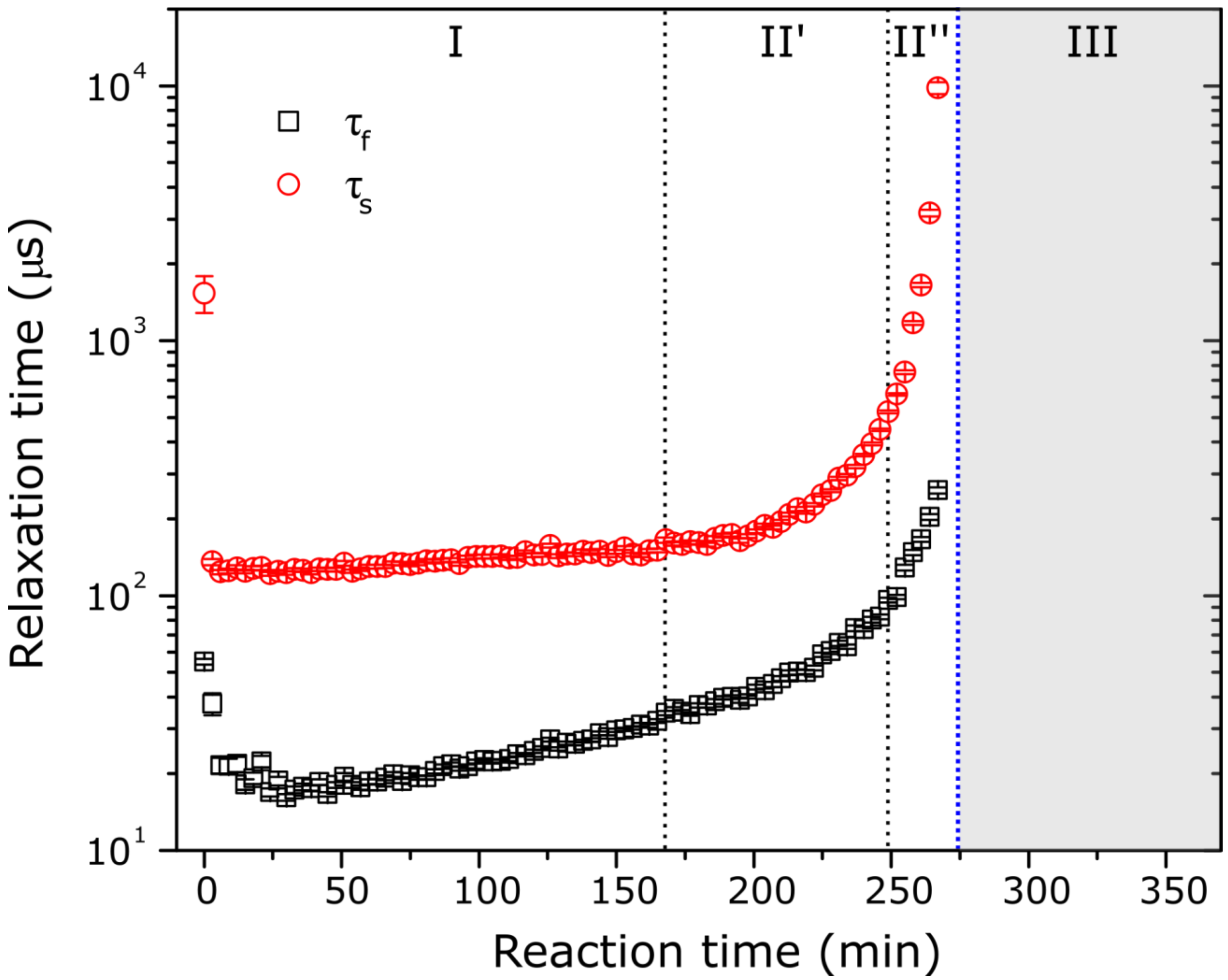

Figure S5. Variation of the correlation length of **1** as function of time during the supramolecular reaction at 80°C. The data were obtained from the fit of the ICF using equation 1 and using equation 2, 3 and 4.

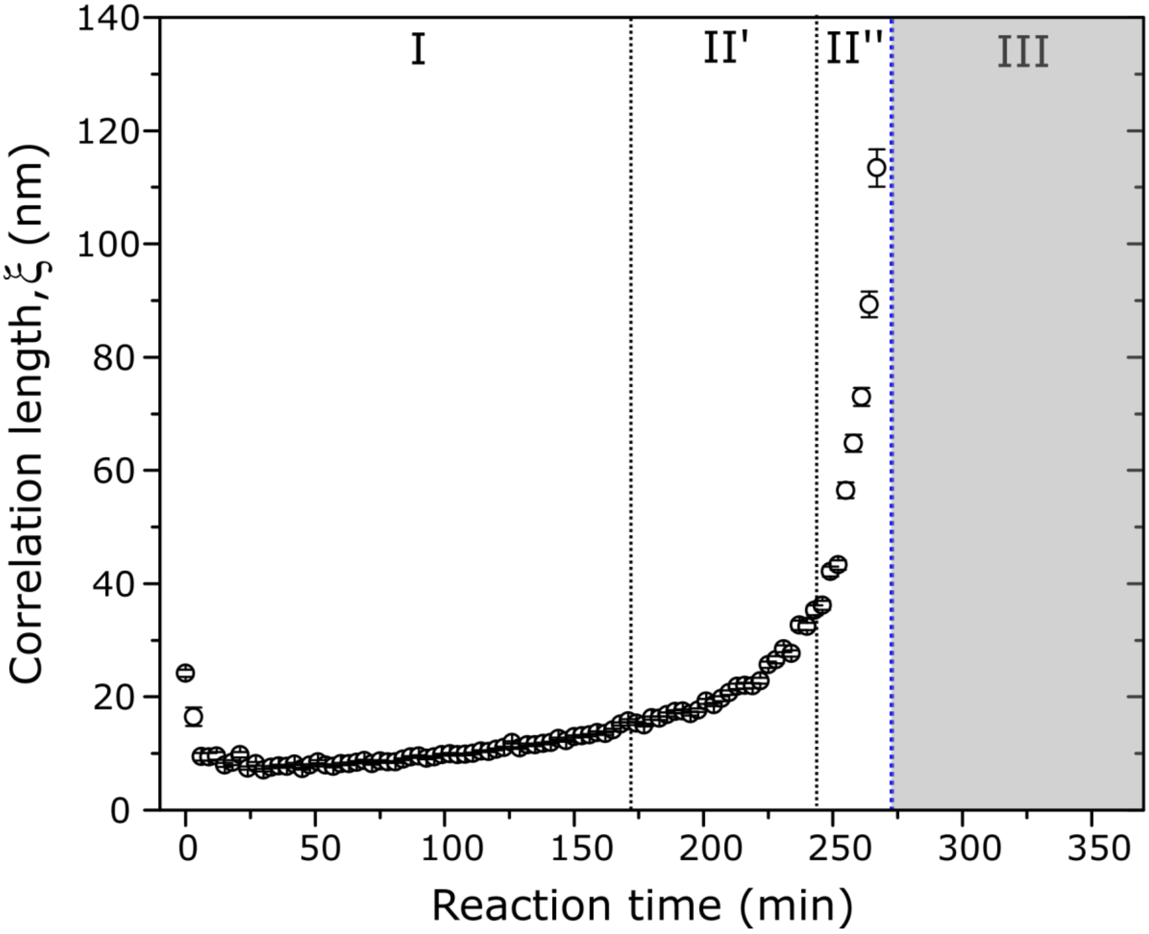

Figure S6. Variation of the correlation length of **1** as function of time during the supramolecular reaction at 80°C. The data were obtained from the fit of the ICF using equation 1 and using equation 2, 3 and 4.

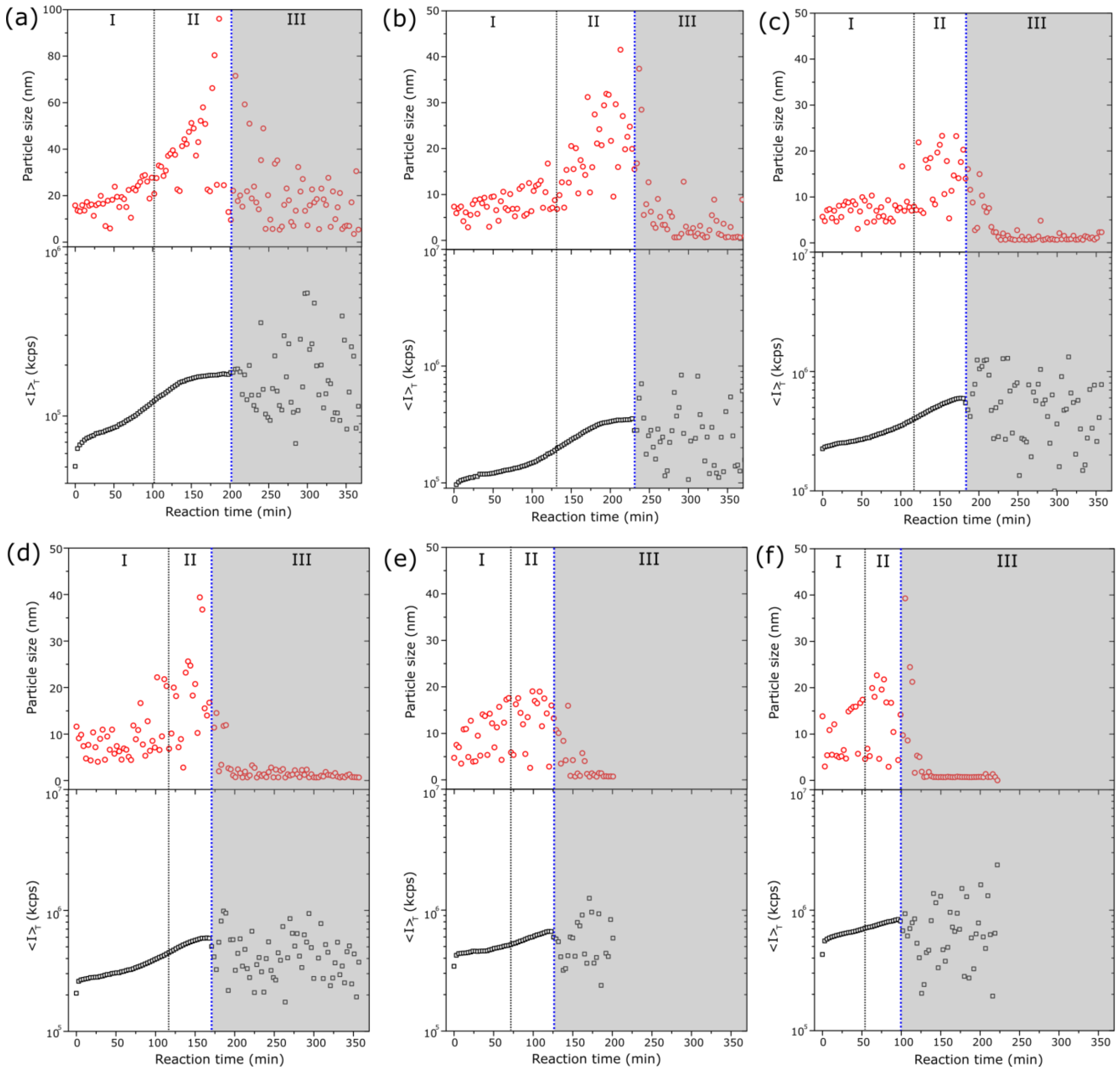

Figure S7. TRDLS measurement during the supramolecular polymerization of **$(C_{12}RhMOP)(bix)_{12}$** at 80°C at a concentration of 0.93 mM, showing the particle size evolution and the time-averaged scattering intensity as a function of time. System with different concentrations were prepared, (a): 0.23 mM, (b) 0.63 mM, (c) 1.37mM, (d) 1.83 mM, (e) 2.20mM, (f) 2.40 mM. The gelation threshold is represented by the blue dotted line. The gray region highlights the effect of the frozen mobility of particles due to gel formation on the DLS response

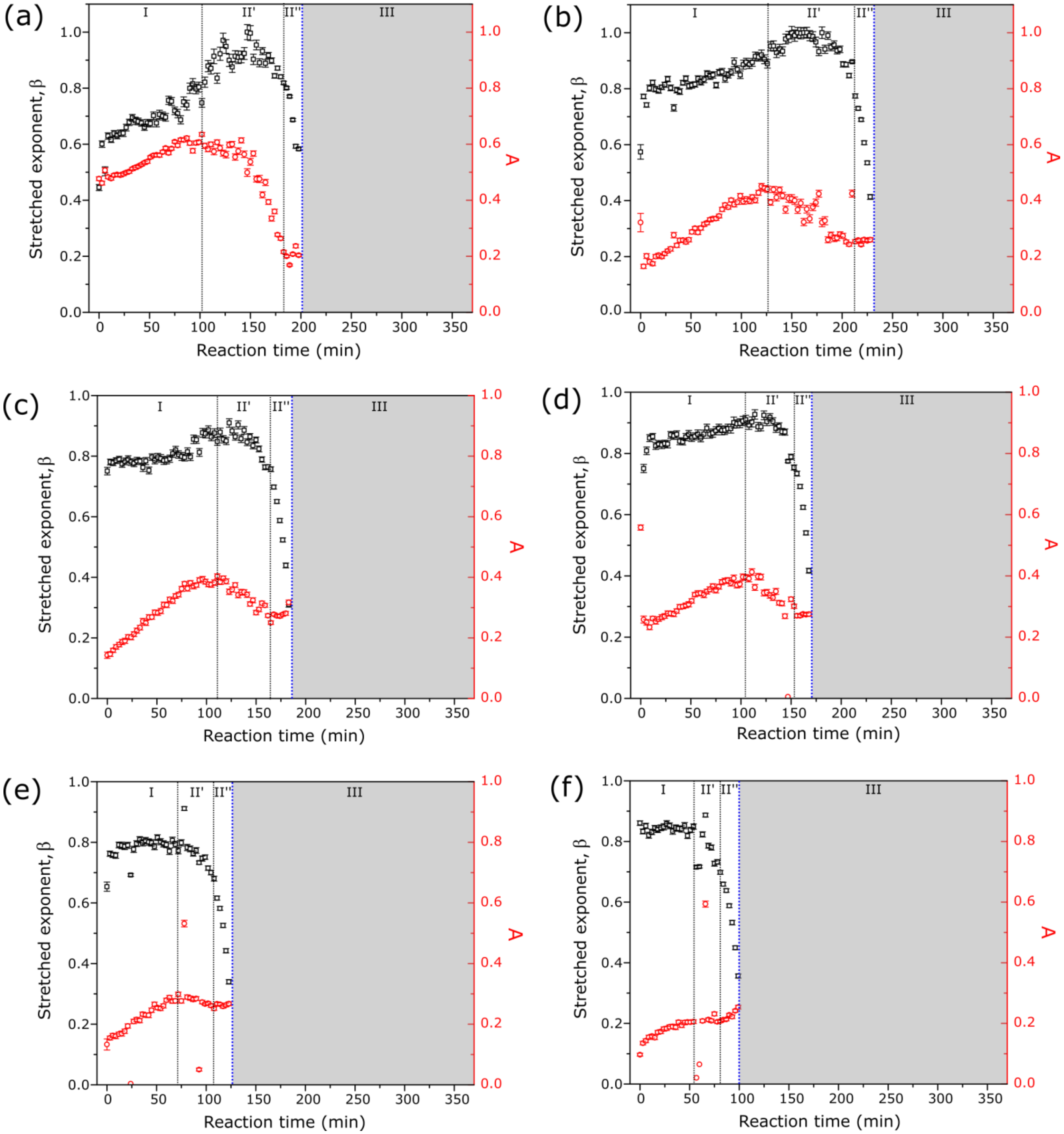

Figure S8. Variation of the fraction of the fast diffusion mode (*A*) and stretched exponent (*β*) as a function of the reaction time for samples prepared with concentration of MOPs of (a) 0.23 mM, (b) 0.63 mM, (c) 1.37 mM, (d) 1.83 mM, (e) 2.20 mM and (f) 2.40 mM.

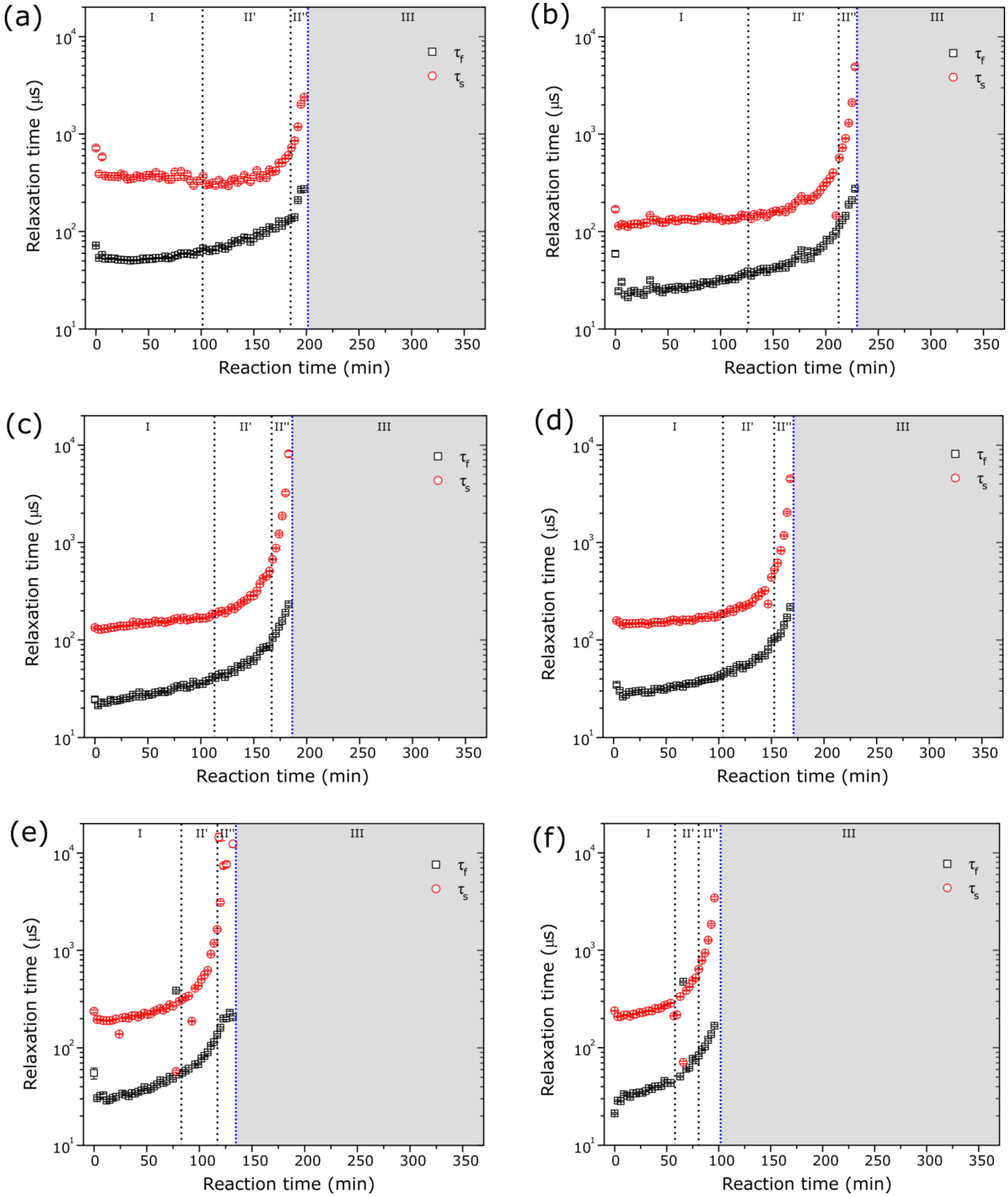

Figure S9. Evolution of the fast (τ_f) and slow (τ_s) relaxation time modes as a function of the reaction time for samples prepared with concentration of MOPs of (a) 0.23 mM, (b) 0.63 mM, (c) 1.37 mM, (d) 1.83 mM, (e) 2.20 mM and (f) 2.40 mM.

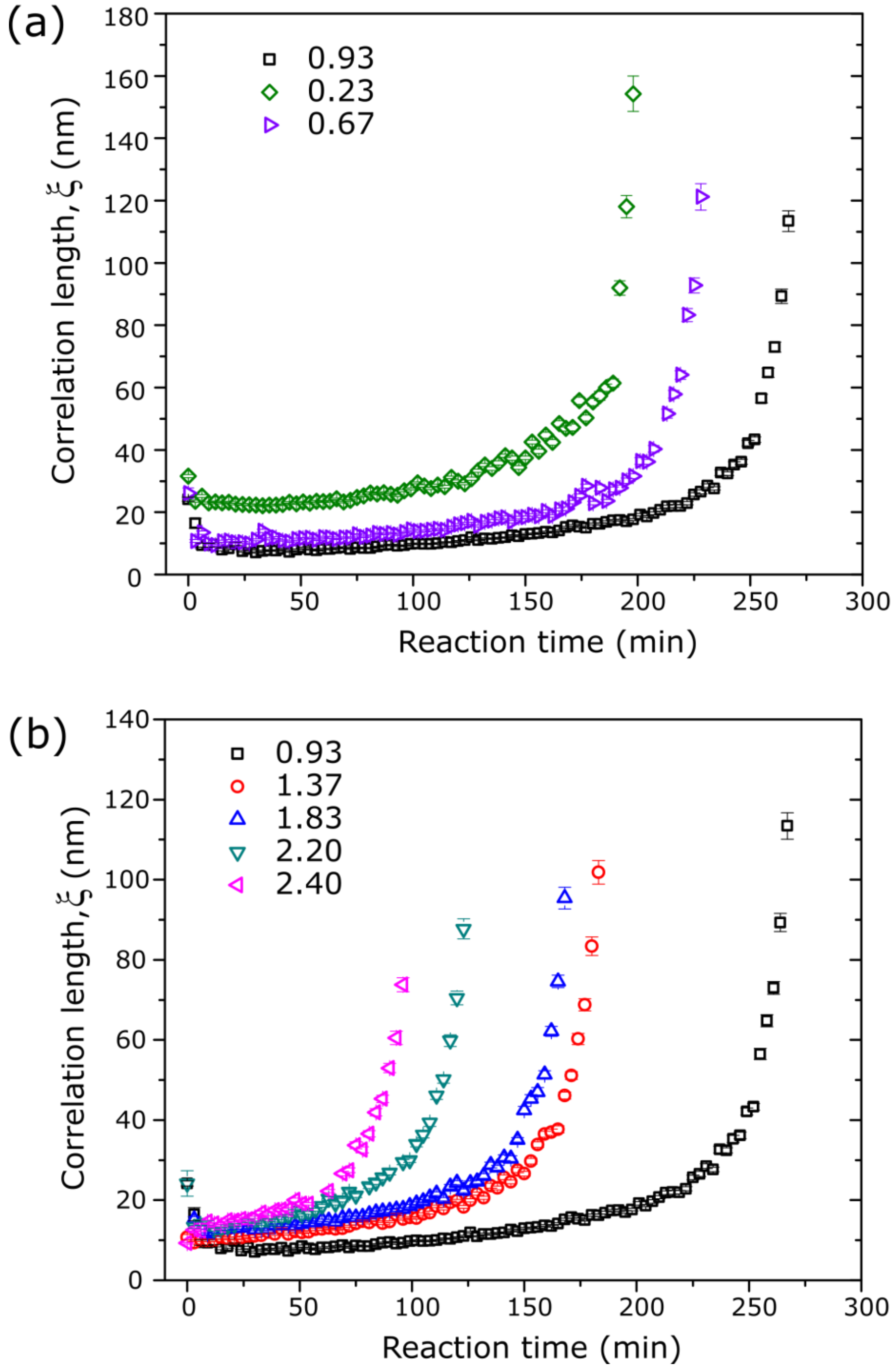

Figure S10. Variation of the correlation length of **1** as function of the supramolecular reaction time at 80°C for different concentration of MOPs. For clarity, samples prepared with a concentration of MOP of 0.23, 0.67 and 0.93 mM are shown in (a) while concentration of MOPS of 0.93, 1.37, 1.83, 2.20 and 2.40 mM in (b). The data were obtained from the fit of the ICF using equation 1 and using equation 2, 3 and 4.

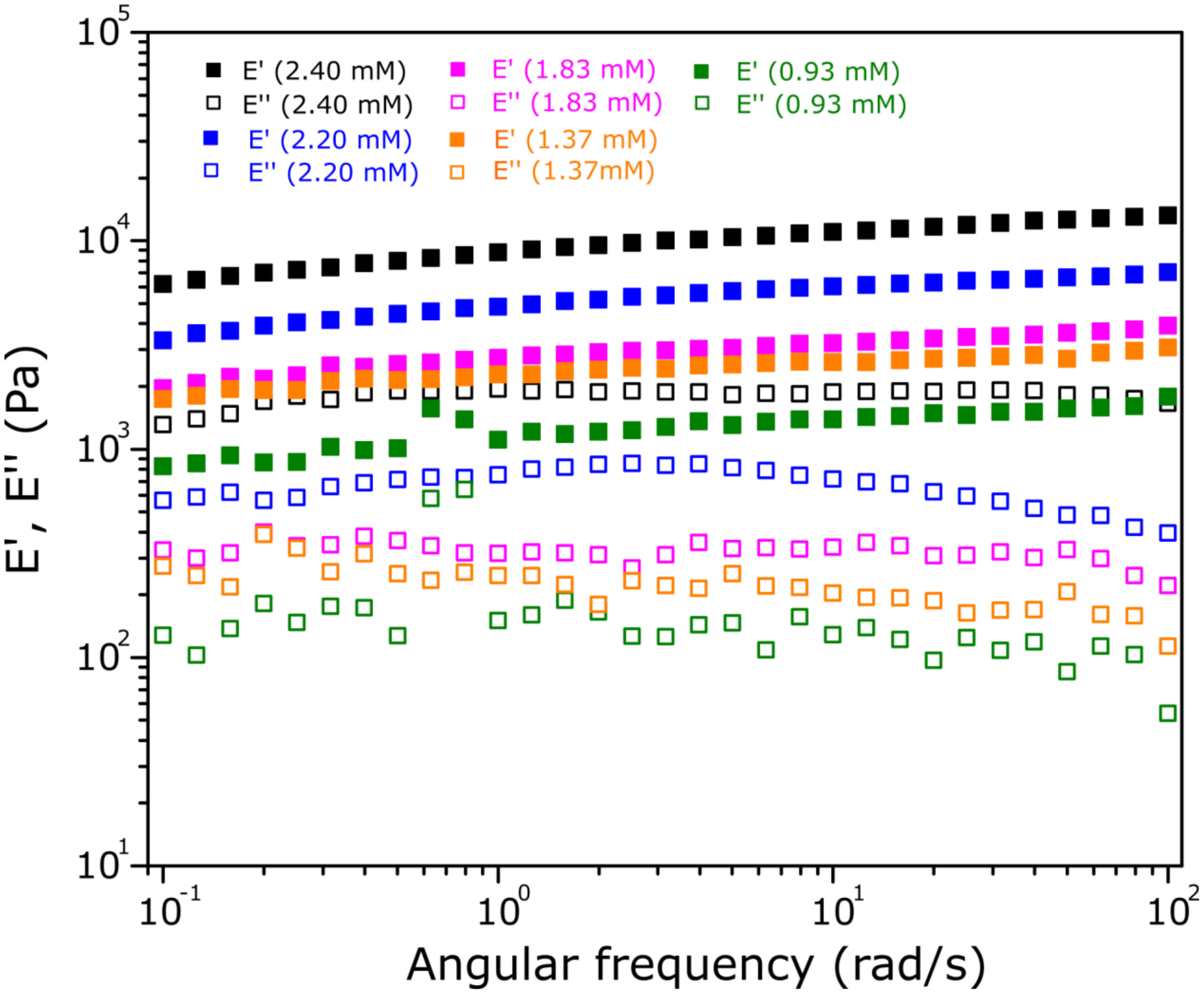

Figure S11. Storage and loss Young's moduli, E′ (close symbol) and E′′ (open symbol) respectively, for gels prepared with concentration of MOP of 2.40 (black), 2.20 (blue), 1.83 (pink), 1.37 (orange) and 0.93 (green) mM. The measurements were performed at a fixed strain amplitude (1%) within the linear viscoelastic regime.

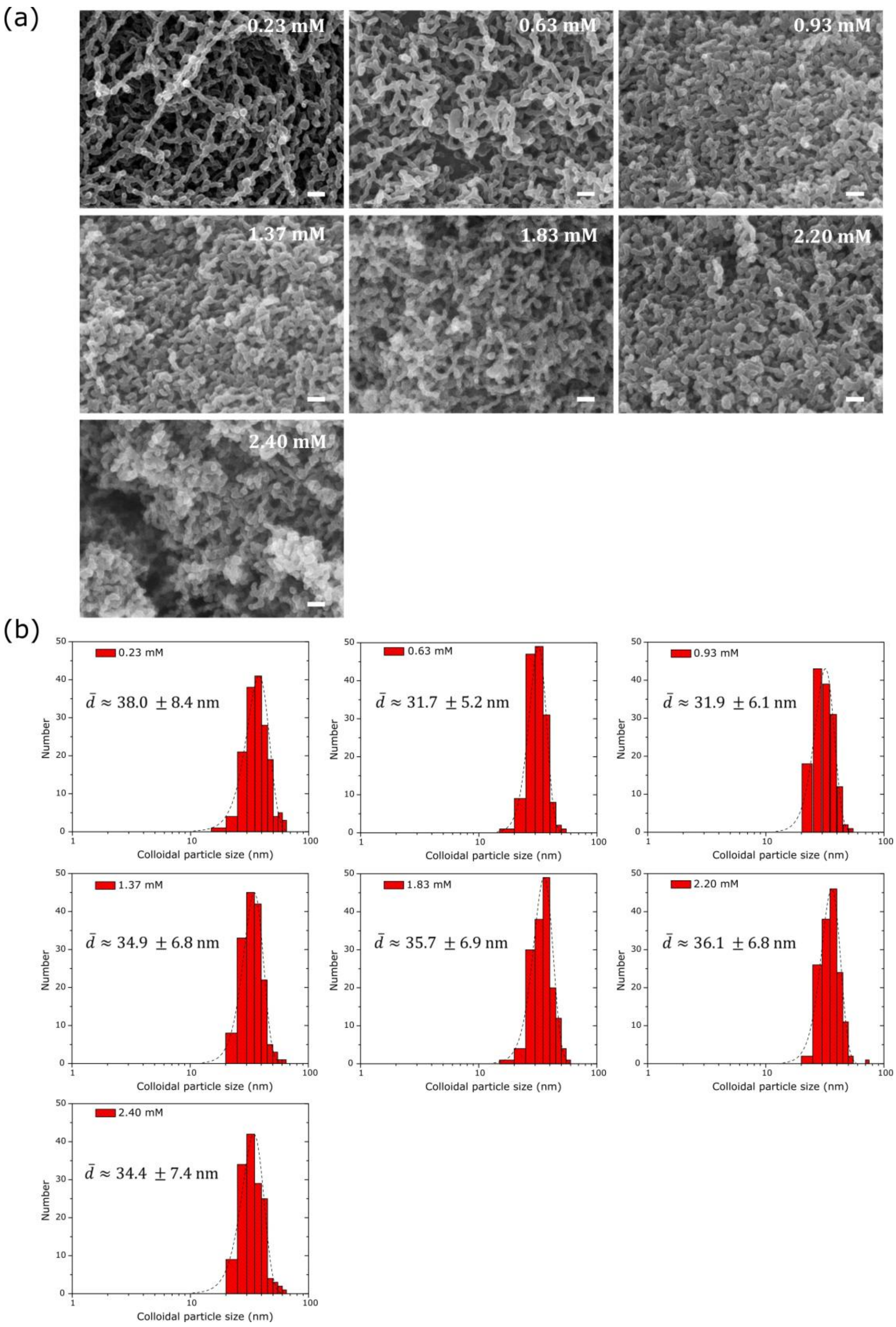

Figure S12. (a) FE-SEM images and (b) the corresponding size distribution of colloid particles determined for the aerogel **2a-g**. The size distributions were obtained from the measurement of 150-160 particle sizes on at least three distinct FESEM images for each sample.

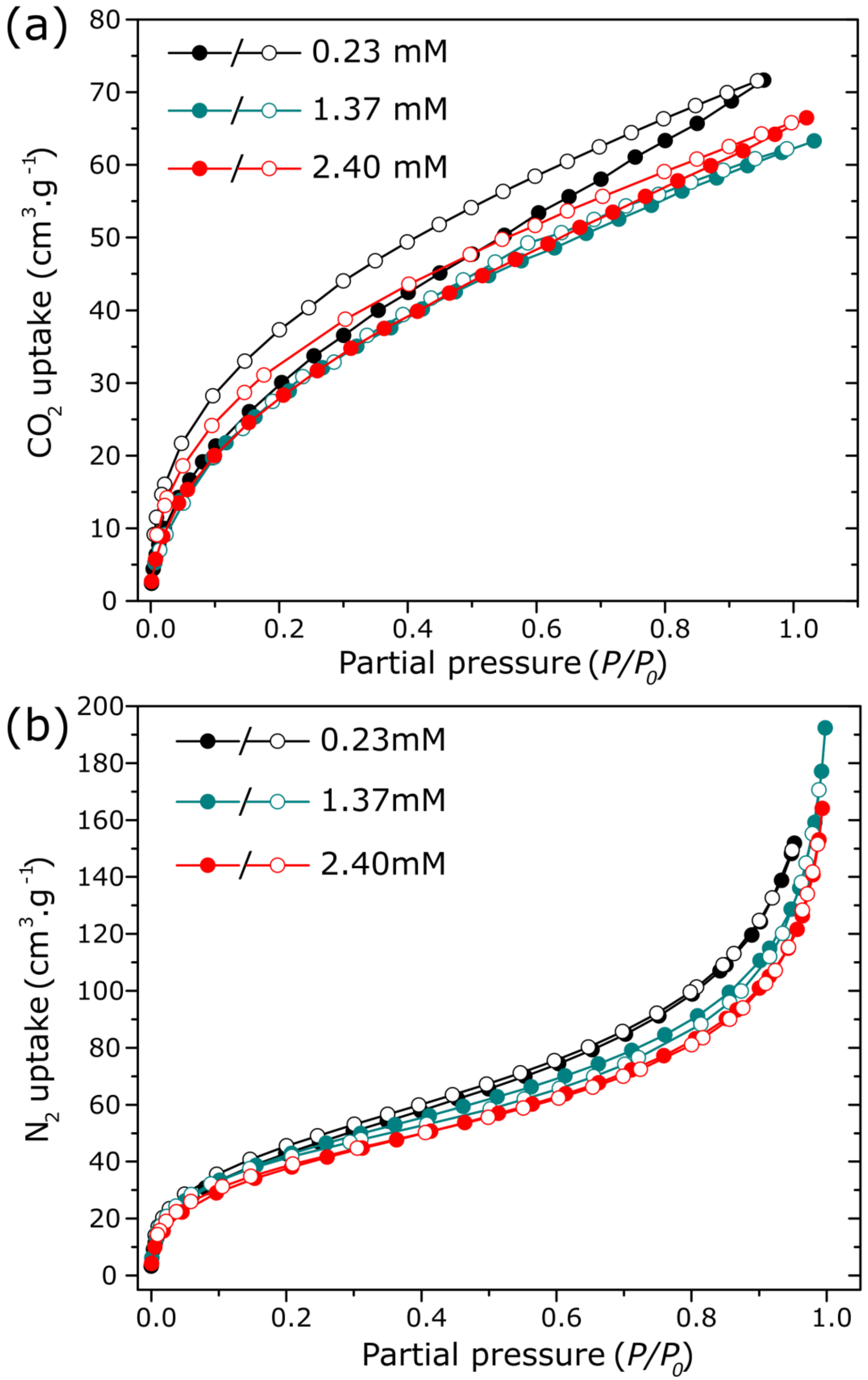

Figure S13. (a) CO_2 uptake (195 K) and (b) N_2 uptake (77 K) for aerogel samples prepared with a concentration of MOP of 0.23 mM (black), 1.37 mM (dark cyan) and 2.40 mM (red).

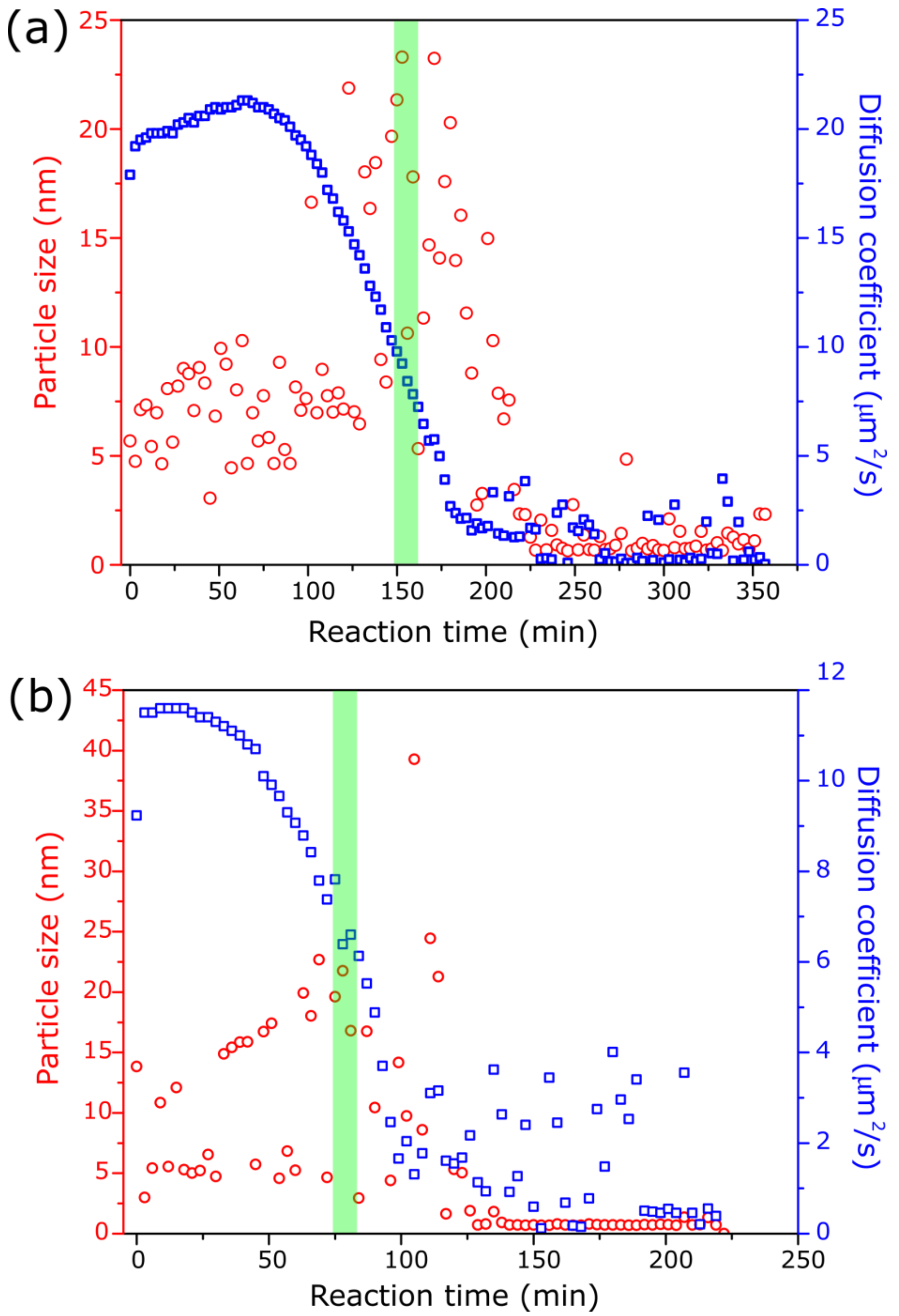

Figure S14. TRDLS measurement during the supramolecular polymerization of **$(C_{12}RhMOP)(bix)_{12}$** at 80°C at a concentration of (a) 1.37 mM and (b) 2.40 mM, showing the particle size evolution and the diffusion coefficient as a function of the reaction time. When the diffusion coefficient reached a value of 7.82 μm^2/s (green region), corresponding to the formation of the colloidal particles, the sample was centrifuged for 5 minutes at 3500 rpm, and then heating was continued for gelation to proceed, yielding the gradient gels **3_{GG}**

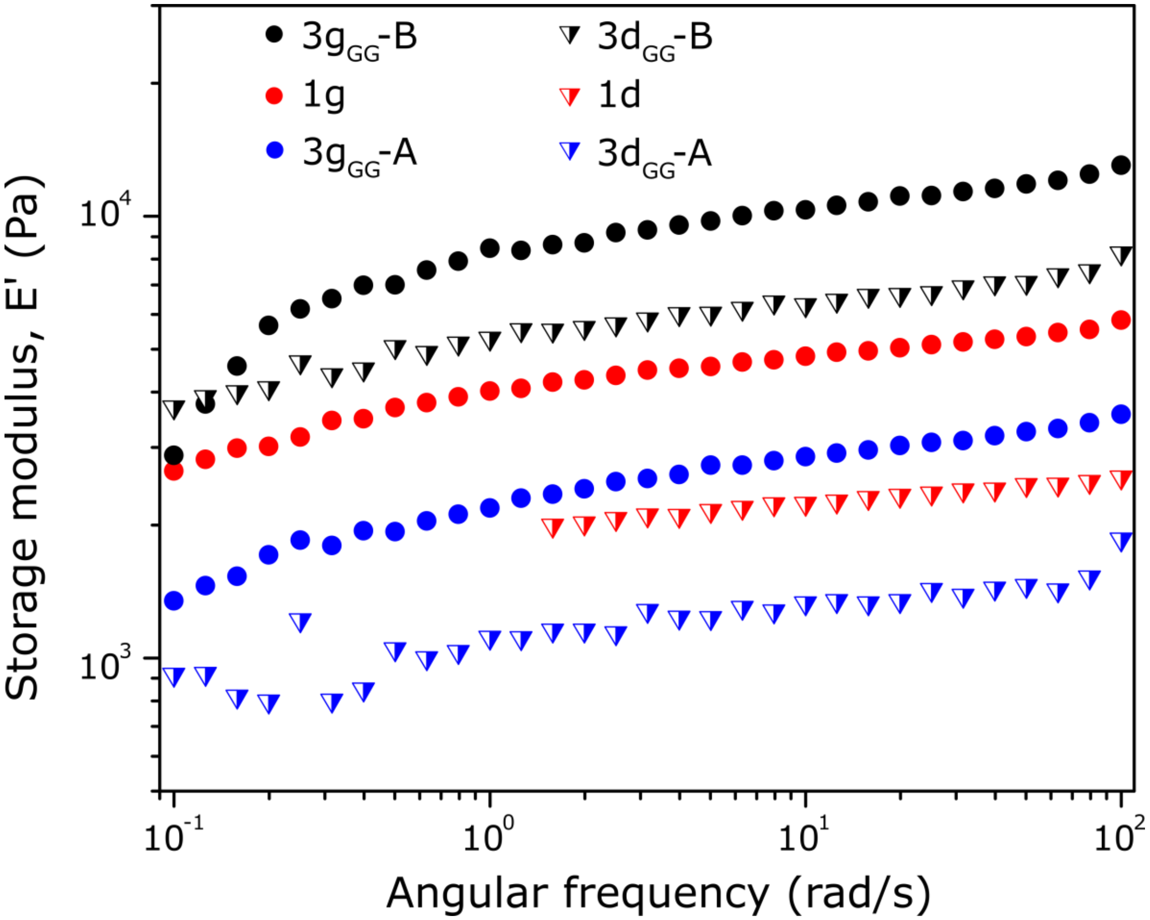

Figure S15. Storage moduli E’ of the bottom (**$3g_{GG}$-B**, black circle and **$3d_{GG}$-B,** black triangle) and top part (**$3g_{GG}$-B**, blue circle and **$3d_{GG}$-B,** blue triangle) of 2.40 and 1.37 mM MOP-based gel prepared using the centrifugation method to create a concentration gradient. As comparison the same gel was prepared without applying centrifugation as reference (2.40 mM, red circle and 1.37 mM, red triangle). The measurements were performed at a fixed strain amplitude (1%) within the linear viscoelastic regime.

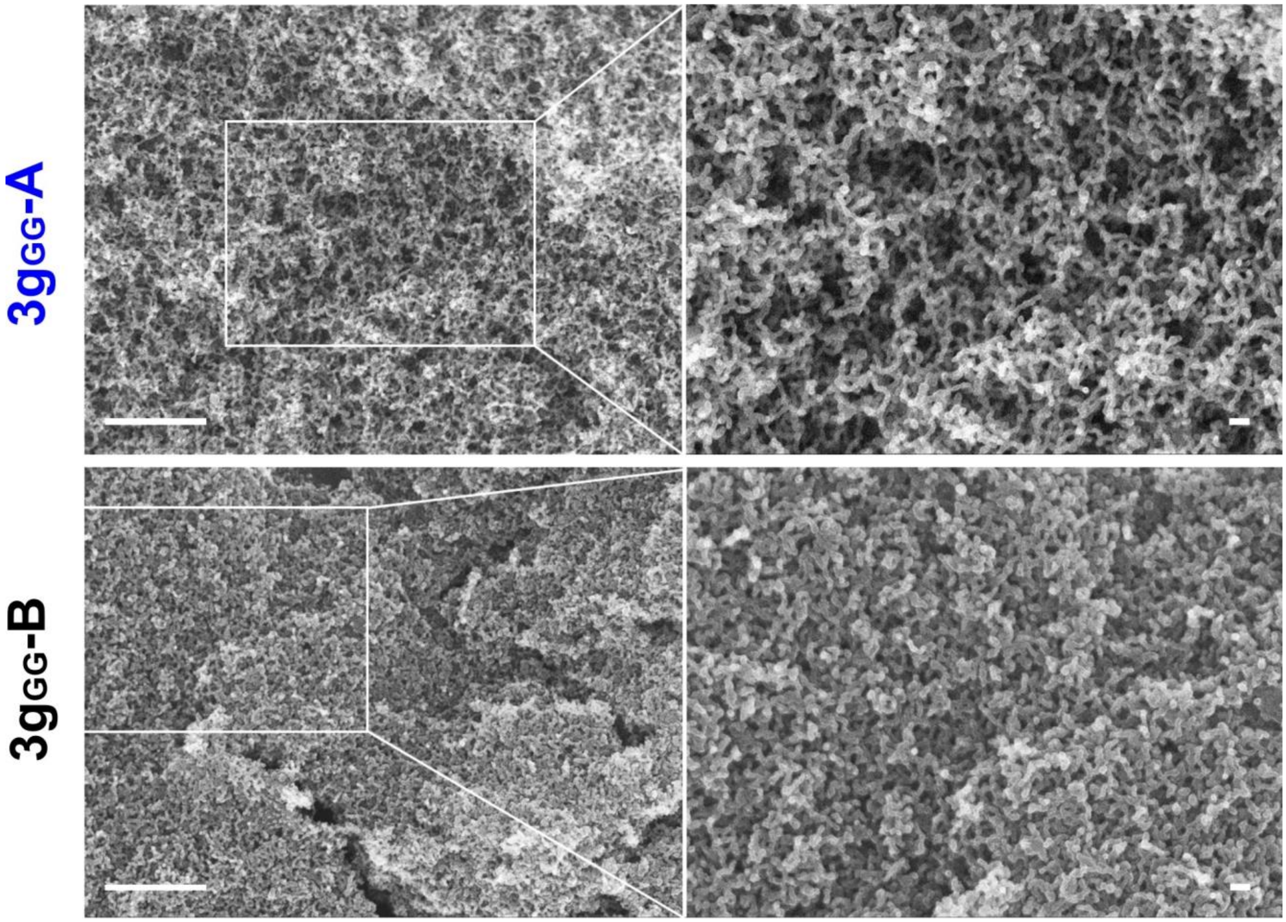

Figure S16. FE-SEM images of the top (**3g$_{GG}$-A**) and bottom part (**3g$_{GG}$-B**) of **3d$_{GG}$** (1.37mM) MOP-based aerogels prepared using centrifugation method. The scale bars for lower and highest magnification are 1 µm and 100 nm, respectively.

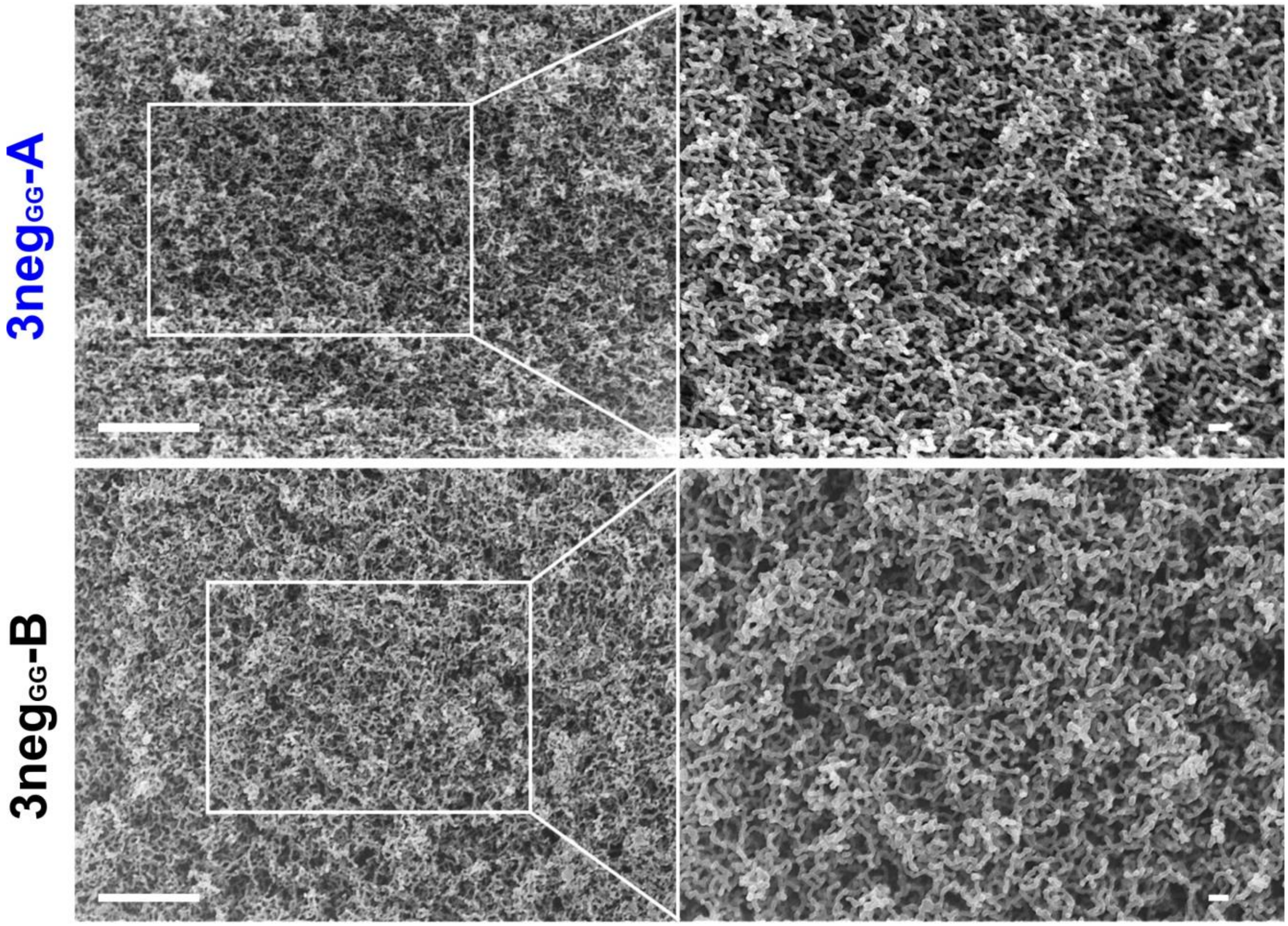

Figure S17. FE-SEM images of the **3neg$_{GG}$** (1.37 mM) MOP-based aerogels prepared using the centrifugation method during the early stage of the supramolecular polymerization (Stage I, t = 60 min) showing the top (3neg$_{GG}$-A) and the bottom (3neg$_{GG}$-B) part of the sample. The right part images are magnification of the corresponding white square. The scale bars for lower and highest magnification are 1 µm and 100 nm, respectively.

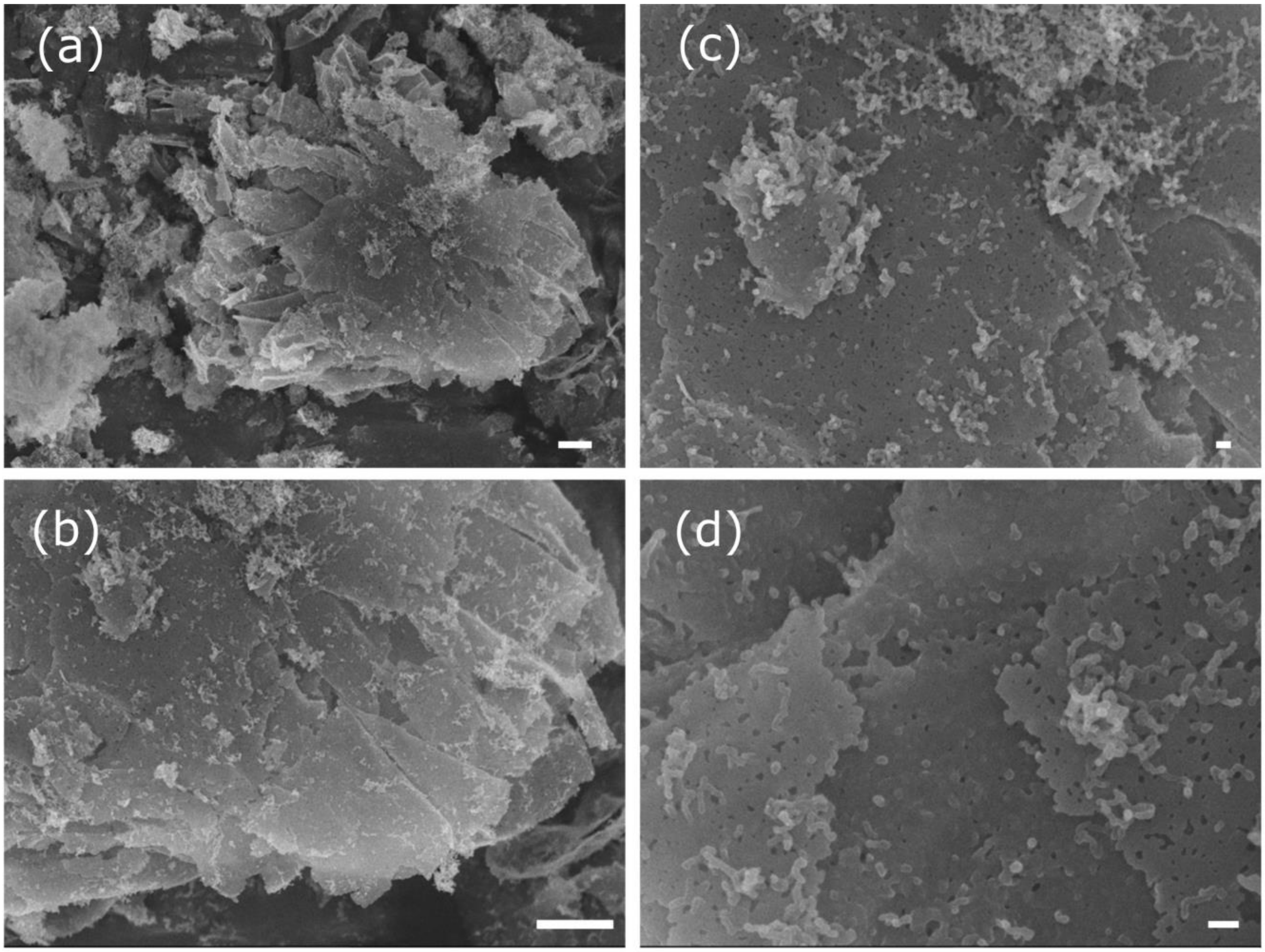

Figure S18. FE-SEM images of the sedimentation part of **3neg$_{GG}$** (1.37 mM) MOP-based aerogels formed when the centrifugation method is applied during the early stage of the supramolecular polymerization (Stage I, t = 60 min) showing different magnification of the sample. The scale bars of (a)-(b) and (c)-(d) are 1 µm and 100 nm, respectively.